Peer Reviewed

Title:

Adaptive optics microperimetry and OCT images show preserved function and recovery of cone visibility in macular telangiectasia type 2 retinal lesions

Author:

Wang, Q
Tuten, WS
Lujan, BJ
Holland, J
Bernstein, PS
Schwartz, SD
Duncan, JL
Roorda, A

Abstract:

Purpose: To evaluate visual function and disease progression in the retinal structural abnormalities of three patients from two unrelated families with macular telangiectasia (MacTel) type 2. Methods: Adaptive optics scanning laser ophthalmoscopy (AOSLO) and AOSLO microperimetry (AOMP)

were used to evaluate the structure and function of macular cones in three eyes with MacTel type 2. Cone spacing was estimated using histogram analysis of intercone distances, and registered spectral-domain optical coherence tomography (SD-OCT) scans were used to evaluate retinal anatomy. AOMP was used to assess visual sensitivity in and around areas of apparent cone loss. Results: Although overall lesion surface area increased, some initially affected regions subsequently showed clear, contiguous, and normally spaced cone mosaics with recovered photoreceptor inner/outer segment (IS/OS) reflectivity (two of two eyes). The AOMP test sites fell within three categories: normal-appearing cones (N), dimly reflecting cones (D), and RPE cell mosaics (R). At N sites, AOMP threshold values (arbitrary units [au]) increased with increasing eccentricity (slope = 0.054 au/degree, r2 = 0.77). The N thresholds ranged from 0.04 to 0.27 au, D thresholds from 0.04 to 0.33 au, and R thresholds from 0.14 to 1.00 au. There was measurable visual sensitivity everywhere except areas without intact external limiting membrane (ELM) and with diffuse scattering in the IS/OS and posterior tips of the outer segments (PTOS) regions on OCT. Conclusions: Visual sensitivity and recovery of cone visibility in areas of apparent focal cone loss suggests that MacTel type 2 lesions with a preserved ELM may contain functioning cones with abnormal scattering and/or waveguiding characteristics. (ClinicalTrials.gov number, NCT00254605.).

Copyright Information:

Adaptive Optics Microperimetry and OCT Images Show Preserved Function and Recovery of Cone Visibility in Macular Telangiectasia Type 2 Retinal Lesions

Qinyun Wang,[1,2] William S. Tuten,[3] Brandon J. Lujan,[3,4] Jennifer Holland,[2] Paul S. Bernstein,[5] Steven D. Schwartz,[6] Jacque L. Duncan,[2] and Austin Roorda[3]

[1]Duke University School of Medicine, Durham, North Carolina, United States
[2]Department of Ophthalmology, University of California, San Francisco, San Francisco, California, United States
[3]School of Optometry and Vision Science Graduate Group, University of California, Berkeley, Berkeley, California, United States
[4]West Coast Retina Medical Group, San Francisco, California, United States
[5]Department of Ophthalmology, University of Utah Moran Eye Center, Salt Lake City, Utah, United States
[6]Jules Stein Eye Institute, University of California, Los Angeles, Los Angeles, California, United States

Purpose. To evaluate visual function and disease progression in the retinal structural abnormalities of three patients from two unrelated families with macular telangiectasia (MacTel) type 2.

Methods. Adaptive optics scanning laser ophthalmoscopy (AOSLO) and AOSLO microperimetry (AOMP) were used to evaluate the structure and function of macular cones in three eyes with MacTel type 2. Cone spacing was estimated using histogram analysis of intercone distances, and registered spectral-domain optical coherence tomography (SD-OCT) scans were used to evaluate retinal anatomy. AOMP was used to assess visual sensitivity in and around areas of apparent cone loss.

Results. Although overall lesion surface area increased, some initially affected regions subsequently showed clear, contiguous, and normally spaced cone mosaics with recovered photoreceptor inner/outer segment (IS/OS) reflectivity (two of two eyes). The AOMP test sites fell within three categories: normal-appearing cones (N), dimly reflecting cones (D), and RPE cell mosaics (R). At N sites, AOMP threshold values (arbitrary units [au]) increased with increasing eccentricity (slope = 0.054 au/degree, r^2 = 0.77). The N thresholds ranged from 0.04 to 0.27 au, D thresholds from 0.04 to 0.33 au, and R thresholds from 0.14 to 1.00 au. There was measurable visual sensitivity everywhere except areas without intact external limiting membrane (ELM) and with diffuse scattering in the IS/OS and posterior tips of the outer segments (PTOS) regions on OCT.

Conclusions. Visual sensitivity and recovery of cone visibility in areas of apparent focal cone loss suggests that MacTel type 2 lesions with a preserved ELM may contain functioning cones with abnormal scattering and/or waveguiding characteristics. (ClinicalTrials.gov number, NCT00254605.)

Keywords: AOSLO, AOMP, MacTel type 2, cone photoreceptors

Macular telangiectasia (MacTel) type 2, also known as idiopathic juxtafoveolar telangiectasia type 2, is a rare bilateral but often asymmetric condition that causes marked visual disturbances, such as impaired reading ability, in patients older than 40 years.[1] Macular telangiectasia type 2 derives its name from the hallmark fluorescein angiography (FA) finding of telangiectatic retinal capillaries temporal to the fovea (Fig. 1).[2–4] Affected eyes also often exhibit photoreceptor inner-outer segment (IS/OS) junction disruptions on optical coherence tomography (OCT).[5,6]

Although the Beaver Dam Eye Study reported the US prevalence of MacTel type 2 as 0.1%, the disease is likely underdiagnosed due to the subtleties of early clinical manifestations as well as late-stage similarity to AMD.[7] Compared with individuals affected by AMD and other eye diseases, those with MacTel type 2 have some of the lowest National Eye Institute Visual Functioning Questionnaire scores.[8,9]

There are neither effective treatments nor reliable measures of disease progression and treatment response, leading to efforts to develop objective structural and functional characterization of the photoreceptors in MacTel type 2. Specifically, confocal adaptive optics scanning laser ophthalmoscopy (AOSLO) compensates for blur-inducing aberrations in the human eye,[10] thereby accurately and noninvasively visualizing macular cone photoreceptor structure to enable measures of cone spacing, density, and packing.[11,12] In MacTel type 2, confocal AOSLO imaging has shown disruption of the normal hexagonal cone mosaic pattern, leading to dark-appearing regions that correlate with characteristic IS/OS junction (or ellipsoid zone band)[13] breaks seen on high-resolution OCT.[14]
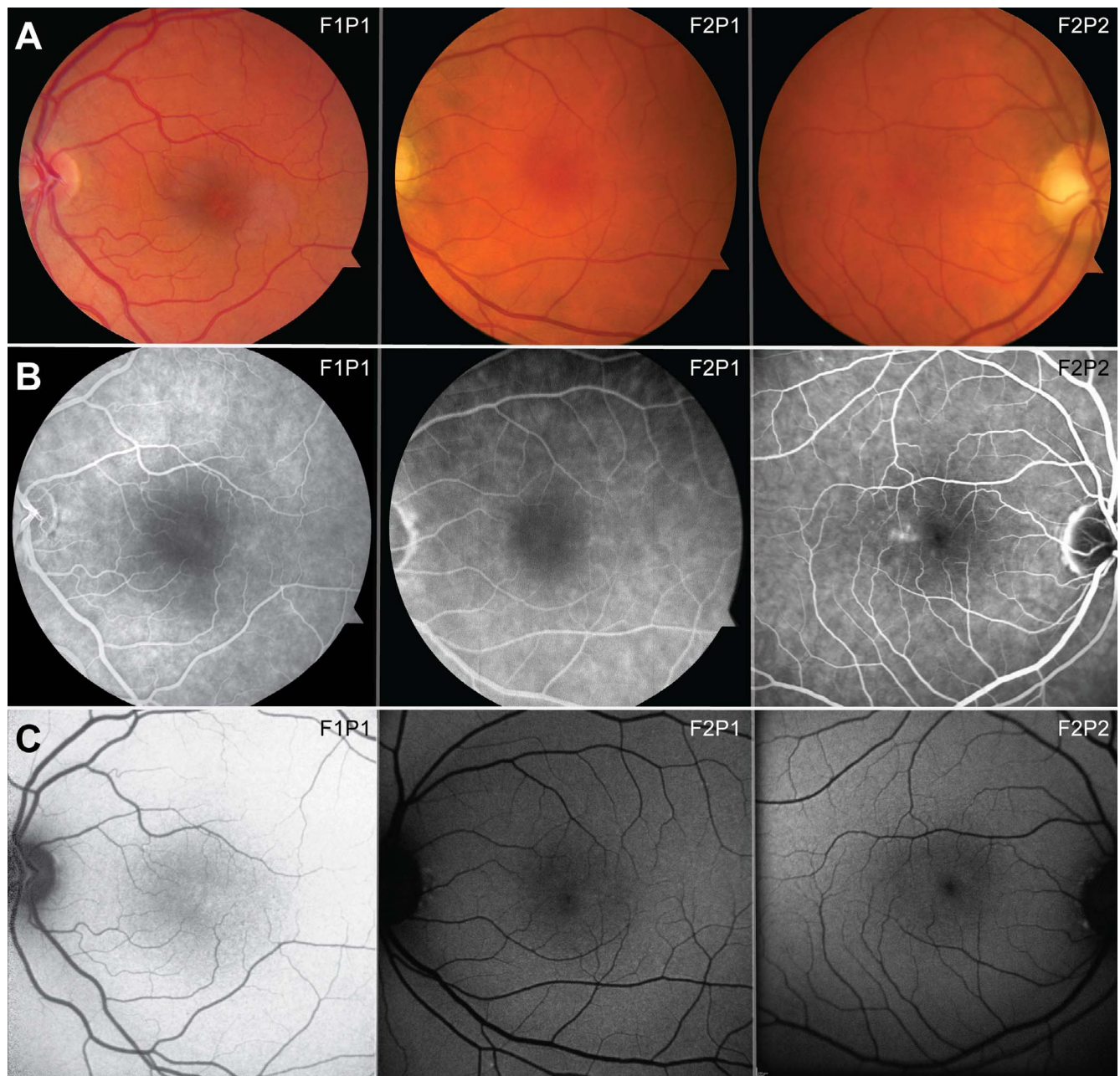
FIGURE 1. Clinical findings in patients with MacTel type 2. Color fundus photos (*row A*) reveal subtle MacTel type 2 features, such as loss of retinal transparency and telangiectatic vessels temporal to the fovea. These are more clearly seen with evidence of hyperfluorescence on FA images (*row B*) and fundus autofluorescence images (*row C*).

Although previous studies have demonstrated visual function abnormalities in MacTel eyes with cone mosaic and IS/OS disruptions,[5,15] standard fundus-guided microperimetry cannot assess retinal function with resolution commensurate with the individual cone structures imaged using AOSLO. Integrating microperimetry into AOSLO makes it possible to concurrently image cones and test their visual function in both an efficient and longitudinal manner.[16] Such an approach, known as AOSLO microperimetry (AOMP), has the potential not only to accurately distinguish between functional and dysfunctional cones in patients with MacTel type 2, but also to assess visual perception in areas of apparent cone loss. This disease is particularly suited to AOMP testing because affected eyes retain healthy retinal regions, allowing patients to serve as their own internal controls.

In this article, we examine cone structure and function in three patients with mild MacTel type 2. We measure the progression of retinal structural changes in two patients and perform AOMP in all three patients at a single time point. The striking result regarding lesion progression is that clear, contiguous, normal-appearing, and normally spaced cone mosaics appear in regions where no apparent cones were present at the first visit. Moreover, we find that some retinal regions lacking both visible cones on AOSLO and structural indicators of cone presence on OCT (IS/OS and posterior tips of the outer segments [PTOS] reflectivity) have residual visual function. Together, these findings suggest that there may be

TABLE. Study Subject Clinical Characteristics

Subject ID	Sex/Age	SE	VA	MR Sphere, Cylinder, Axis	Time Since BL	Area of IS/OS Loss on En Face OCT	FH MacTel, Yes/No
F1P1	F/43	OS	BL: 20/16 FU: 20/32	−0.50 diopter sphere	2 y	BL: 0.14 mm^2 FU: 0.17 mm^2	No
F2P1	F/49	OS	BL: 20/20 FU: 20/16	+1.25 +0.25 × 016	4 y	BL: 0.04 mm^2 FU: 0.28 mm^2	Yes
F2P2	M/52	OD	BL: 20/20	Plano	N/A	N/A	Yes

Information includes patient sex (F, female; M, male), age at most recent study (years), study eye (SE), VA, manifest refraction (MR), and family history (FH). BL, baseline; FU, follow-up; N/A, not applicable.

some functional intralesion cones that have the potential to recover normal scattering characteristics. An indicator of these reclaimable cones may be an intact external limiting membrane (ELM) that has a relatively transparent and uncollapsed retinal structure beneath it.

MATERIALS AND METHODS

Participants

Three subjects with MacTel type 2 were enrolled at the University of California, Berkeley, after the diagnosis of MacTel type 2 was confirmed at the Moorfields Eye Hospital Reading Center (London, UK). Informed consent was obtained after the study protocol and its associated risks were reviewed with each subject. The informed consent forms and study protocol were approved by the University of California San Francisco, University of California Berkeley, University of California Los Angeles, and University of Utah Institutional Review Boards, and research procedures followed the tenets of the Declaration of Helsinki.

The participants were two women and one man from two unrelated families (F1P1, F2P1, and F2P2; Table). Participants F1P1 and F2P1 were imaged at two time points (Table), but only structural imaging was done at visit one, as the technology for AOMP had not been developed at the time. In the past year, all three patients were brought in for AOMP and imaging. The study eye in each patient was selected based on clarity of OCT and AOSLO image quality.

Enrollment inclusion criteria included being 18 years of age or older with signs of MacTel type 2, visual acuity of at least 20/40 in either eye, clear ocular media (cornea and lens), and fixation stability (ability to fixate for at least 15 seconds).

Clinical Measures

All subjects had undergone complete eye examinations by retinal specialists (PSB, SDS) within a few months of study enrollment. Clinical information gathered at these visits included best-corrected visual acuity, color fundus photographs, FAs, and fundus autofluorescence images (F1P1: HRA2 system; F2P1 and P2P2: Spectralis HRA+OCT system [Heidelberg Engineering, Vista, CA, USA]). The study eyes are shown in Figure 1.

For each study eye, pupil dilation was achieved with one drop of 1% tropicamide and one drop of 2.5% phenylephrine. Frame-averaged line scans, each composed of 20 individual B-scans, were acquired with one of two Cirrus HD-OCT (Carl Zeiss Meditec, Inc., Dublin, CA, USA) retinal imaging systems. Macular cube volume scans were acquired with either the commercially available 512 × 128 cube protocol covering 6 mm^2, or a proprietary 256 × 256 cube protocol covering 3

mm^2. A line-scanning ophthalmoscope integrated into the Cirrus system obtained infrared fundus scans simultaneously with the spectral-domain (SD)-OCT acquisition and was used to indicate scan position.

En face OCT scans were derived from IS/OS slabs that were between 43 and 45 μm thick, and a significant reflectivity decrease in these scans indicated a disruption of the normal IS/OS. The surface area of these defects was measured via ImageJ (http://imagej.nih.gov/ij/; provided in the public domain by the National Institutes of Health, Bethesda, MD, USA) (Table).

Adaptive Optics Scanning Laser Ophthalmoscopy Imaging and AOMP Testing

High-resolution AOSLO images were obtained from each study eye using an AOSLO as previously described.[17–19] Individual AOSLO images, which covered 1.2° × 1.2° of retina, were assembled into larger montages that encompassed the fovea, the macular area with IS/OS junction band disruption, and surrounding normal cones in each imaged eye. An attempt was made to image the photoreceptor mosaic at every location. At locations where the photoreceptor mosaic was not visible, but the RPE mosaic was visible (corresponding to a complete break in the IS/OS layer in OCT), we adjusted the focus slightly deeper to improve resolution of the RPE mosaic. As such, the montages do not necessarily represent an image from a single depth plane in the retina. The appearance of the images in the immediate vicinity of the lesions fell into three categories:

- N: normal-appearing cone mosaics on AOSLO, presence of normal-appearing ELM, IS/OS, and PTOS on OCT.
- D: weakly reflecting or no cones visible on AOSLO; presence of ELM, IS/OS, and PTOS, but IS/OS and PTOS appear relatively dim or disrupted.
- R: RPE cells, but no cone mosaic is visible on AOSLO; IS/OS and PTOS are not present, ELM may or may not be present.

Using information shown in SD-OCT images and AOSLO montages, specific 0.1° × 0.1° retinal regions of interest were manually selected for AOMP functional testing. The AOMP tests were done at N, D, and R sites, all of which were located between 0 and 185 arcminutes (0° and 3.1°) from the preferred retinal locus (PRL), presumed to be the anatomical fovea (Matlab; MathWorks, Natick, MA, USA). The method of identifying the PRL is described in a previous paper.[20] The N category AOMP test sites across all three eyes provided normative data against which thresholds values in all eyes were compared.

The AOMP was implemented via custom software used for programming psychophysical experiments at the University of California Berkeley (Matlab; MathWorks). The AOSLO light source was a supercontinuum laser (SuperK EXTREME; NKT
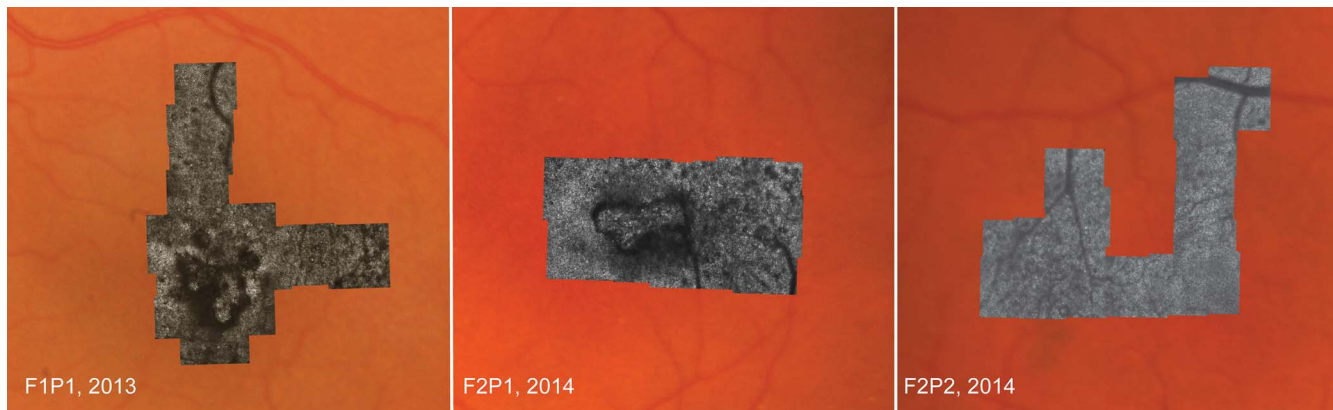
FIGURE 2. Relative location and size of MacTel type 2 lesions studied with AOSLO montages superimposed on clinical images. In F2P2, the patient with earliest disease, telangiectatic vessels temporal to the fovea and inner retinal microcysts are the only abnormal findings.

Photonics, Inc., Birkerød, Denmark) whose broadband output was passed through serial edge and narrowband filters to produce independent imaging ($\lambda = 840$ nm) and stimulation ($\lambda = 543$ nm) channels, each of which could be controlled by high-speed acousto-optic modulators (Brimrose Corporation, Baltimore, MD, USA).[16] The stimulation wavelength was selected on the basis that it drives L and M cones, which make up 90% to 95% of the cone receptor mosaic, equally.[21] The stimulus diameter was roughly half that of a Goldmann I-sized stimulus (3.45 arcminutes or 0.05°), and its area would span between 43 (at the fovea) and 5 (at 3°) cones in a normal retina.[22] To ensure accuracy of stimulus delivery to a given AOMP test site, locations were visualized using dynamic AOSLO imaging and tracked by a high-speed image-based eye-tracking algorithm, which predicted the precise moment to deliver the stimulus.[23] Longitudinal chromatic aberration was corrected according to published levels and is expected to be accurate to better than 0.1 diopter.[24] Additionally, transverse chromatic aberration (TCA) was measured and corrected according to established methods when image quality permitted[25]; in other cases, the TCA was minimized subjectively by asking the subject to fixate the imaging and stimulus rasters, then adjusting pupil position until the two were brought into alignment. For all test sites, the focus of the stimulus was maintained on the photoreceptor mosaic. For the D and R sites, the focus was set so that the photoreceptor mosaic outside of the tested area, but within the imaged field, was in best focus.

Visual sensitivity was assessed via an increment threshold approach. Light leaking through the stimulus channel provided a background of approximately 4 cd/m², bright enough to prevent rod photoreceptors from contributing to the measured thresholds. Stimulus intensity was represented in arbitrary units (au) on a linearized scale from 0 to 1 (a value of 0 indicates the presence of the background only; an intensity of 1 represents the strongest light the system is capable of presenting); when the acousto-optic modulator background is set to approximately 4 cd/m², the full intensity of the stimulus is approximately 2700 cd/m², which is nearly as bright as the brightest Humphrey stimulus (3174 cd/m² = 10,000 apostilbs). The AOMP results were generated using a subject-paced 4- to 2-dB staircase with yes-no response paradigm.[26] At each AOMP test site, the subject pushed a button to initiate a staircase, which typically consisted of 12 to 15 trials and was repeated three times per retinal test site. A trial involved the following sequence of events: successful stimulus delivery, signaled by an auditory cue; subject's "yes" or "no" keyboard response; subject's initiation of the next trial. Trials with failed stimulus delivery were repeated immediately, and each retinal test site underwent a total of 36 to 45 trials.

Image Overlays

Comprehensive image overlays were generated (Adobe Illustrator; Adobe Systems, Inc., San Jose, CA, USA) to contextualize OCT, AOSLO, and AOMP measures. The AOMP retinal test sites were marked on respective AOSLO montages, which were then correlated precisely with clinical images demonstrating the MacTel type 2 lesions (Fig. 2). En face OCT slab images of IS/OS layers and single cross-sectional OCT B-scans, along with corresponding scan lines, were subsequently superimposed on AOSLO montages and precisely registered using the study eye's lesion appearance and vascular anatomy.

Cone Spacing

Cone spacing was measured at locations with unambiguous arrays of contiguous cones and avoided where cones may have been obscured by inner retinal pathology. Using the methods previously described,[19,27] cone spacing was estimated via custom software (Matlab; MathWorks), which extracts the nearest neighbor distance based on a histogram of all intercone distances from subsets of cones at 43 locations, all of which showed unambiguous cones and were in the N category. Study eye values were compared with values from 27 age-similar healthy eyes. Selected locations included 10 of the 13 N category AOMP test sites.

Statistical Methods and AOMP Data Analysis

Among the three study eyes, a total of 22 retinal test sites were tested using AOMP; 13 of these 22 sites were in the N category, 4 in the D category, and 5 in the R category. During AOMP testing, an individual retinal site generated a series of thresholds (au) that were averaged into a single value. Linear regression analysis of N site thresholds across all three eyes was used to determine expected threshold values for normally functioning cones at any given eccentricity. A P value less than 0.05 was considered to be statistically significant.

RESULTS

Progression

For study eyes F1P1 and F2P1, comparison of current and previous AOSLO montages showed expansion of lesion
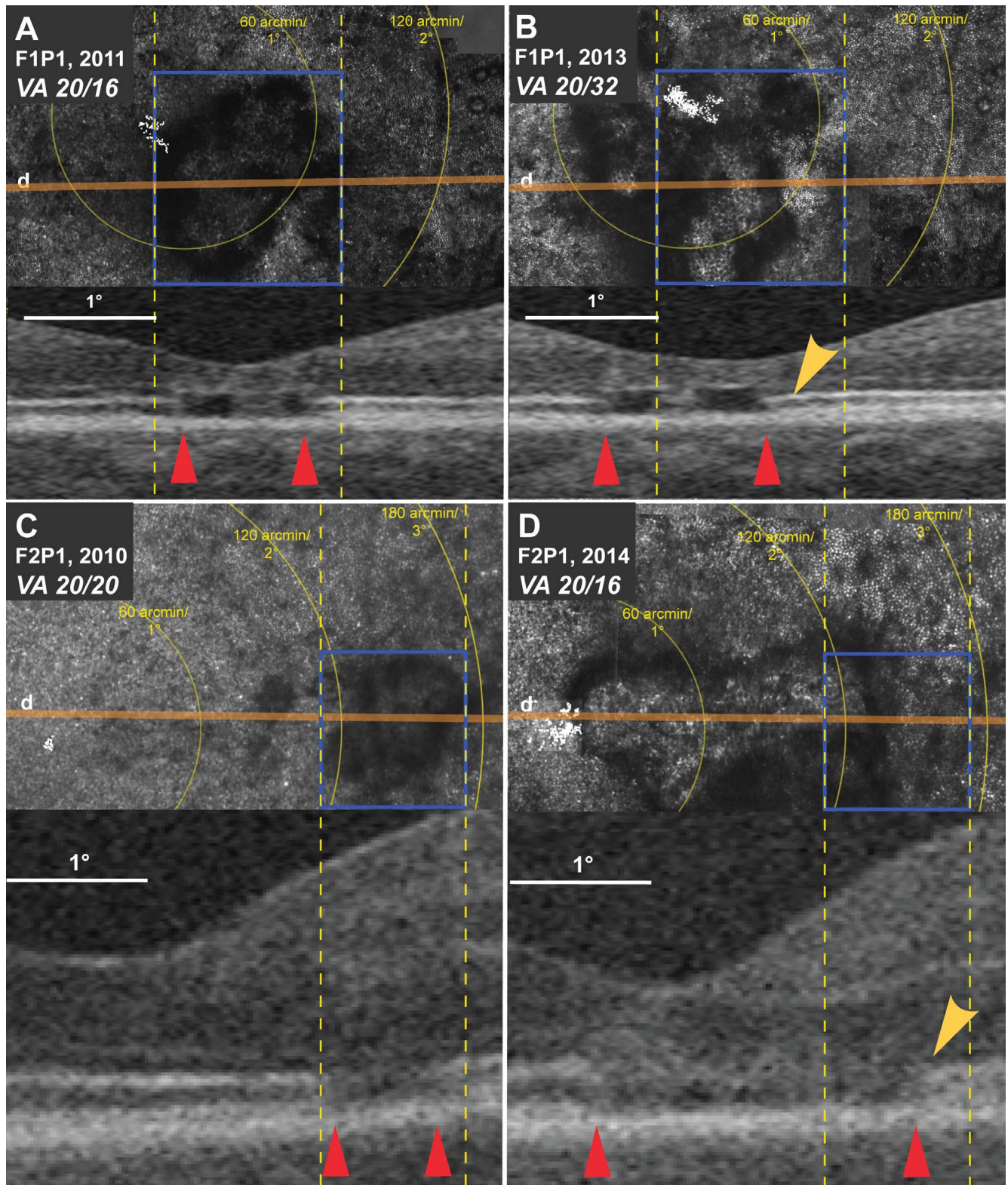
FIGURE 3. Disease progression in two MacTel type 2 patients. Baseline lesion boundaries are outlined in *blue* on AOSLO and correlated with OCT B-scans via *yellow, vertical dashed lines*. *Tan lines* indicate location of OCT B scans shown below each AOSLO montage. Visual acuity, PRL (*white clusters*), and IS/OS breaks on OCT (*red arrowheads*) are shown. (**A, B**) AOSLO (*top row*): There is nasal expansion from 2011 to 2013. Within the *blue rectangle*, there are newly resolvable, hyperreflective cones temporally that are not seen in (**A**). OCT (*bottom row*): Selected scan shows anatomy at all three AOSLO-defined categories (N, D, R). The reflectivity of the IS/OS line within the lesion is relatively dim compared with outside the lesion. In (**A**), the *dashed vertical lines* do not correspond exactly with IS/OS breaks. In (**B**), the same *dashed lines* show that temporally, a small, previously dark IS/OS segment in 2011 is hyperreflective in 2013 (*yellow arrow*). VA, PRL: The decline in VA coincides with a shift in PRL. (**C, D**) AOSLO: There is nasal extension from 2010 to 2014. Within the *blue rectangle*, there are apparent cones in a formerly dim region temporal to the vertical retinal vascular landmark. OCT: The IS/OS defect has increased and extended nasally. A small, previously dark IS/OS segment in 2010

appears hyperreflective in 2014 (*yellow arrow*). Note: The difference in foveal contours between (**C**) and (**D**) is likely due to loss of outer retinal layers, as demonstrated in Figure 4B, B-scans a through e. VA, PRL: VA stable, PRL center unchanged during the course of the study.

boundaries (Table). In F1P1, the lesion expanded nasally to include the original PRL, forcing the subject to adopt a slightly eccentric PRL (Figs. 3A, 3B). This eye also experienced a decrease in visual acuity (VA) from 20/16 to 20/32 (Table). In F2P1, the lesion, which at the first visit started 2° temporal to fixation, expanded nasally to reach the anatomical fovea (Figs. 3C, 3D). The PRL and acuity in this patient remained stable between visits.

The most striking change was that in both F1P1 and F2P1, subsequent visits showed clear and contiguous arrays of cones in some previously affected intralesion regions. The OCT images showed corresponding recovery of the reflections, consistent with the IS/OS junction and the PTOS (Figs. 3A–D).

Structural Characterization

At 41 of 43 locations where unambiguous cones were observed (10/41 were AOMP N sites), cone spacing values fell within the 95% confidence interval of the normal mean, which was calculated using values from 27 healthy eyes. These normally spaced locations included four areas within newly resolvable cone arrays. The remaining 2 of the 43 locations had spacing values in the 99% confidence interval.

In F1P1 and F2P1, en face OCT slab images containing the IS/OS showed dark MacTel type 2 lesions that correlated well with lesions seen on corresponding AOSLO montages. On cross-sectional OCT B-scans, the reflectivity of the IS/OS lines within the lesions were relatively dim or absent compared with outside the lesions. The B-scans in F1P1 (Fig. 4A, white arrowheads, scans e and f) revealed a relatively preserved ELM line with a highly transparent posterior section where the IS/OS and PTOS are normally seen, whereas in F2P1 these distinctions were less clear (Fig. 4B, white arrowhead, scan c). In F2P2, there was no discontinuity in the cone mosaic, IS/OS, or ELM, although shadows of inner retinal abnormalities were seen in the AOSLO montage (Fig. 4C) and telangiectatic vessels were observed temporal to the fovea on FA (Fig. 1B).

Functional Characterization

The AOMP thresholds measured at all 13 N sites increased with increasing eccentricity (Fig. 5; slope = 0.054 au/degree, R^2 = 0.77, $P < 0.0001$), demonstrating that for normal-appearing cones, visual sensitivity decreases with increasing distance from the fovea at a similar rate for all three subjects.

All 9 AOMP test sites in the D and R categories were measured in subjects F1P1 and F2P1, whereas the third study eye (F2P2) had only N category retinal test sites (Figs. 4A–C). Of four D sites tested in regions with dimly reflecting cones, three produced average threshold values at least 2-fold greater than normal, corrected for eccentricity. Of the five R sites tested where RPE cells were visible, average threshold values were at least 2-fold greater than normal at three sites and at least 4-fold greater than normal at the other two (Fig. 5).

Discussion

This is the first report of recovered visibility of contiguous cone arrays within regions that had previously been identified as being within a lesion. This is also the first report showing measurable function in recovered regions as well as regions where no cones were visible on either OCT or AOSLO imaging. These new findings have challenged our notion that regions with no visible cones on OCT or AOSLO lacked cones as well as visual function, leading to the following questions:

1. Cone structure: What is the nature of cone visibility recovery? Are cones migrating into this region; are new cones forming; or does this reflectivity recovery come from cones that were always present?
2. Cone function: What is the best explanation for the existence of light sensitivity in areas where no cones are visible on AOSLO and that lack visible structures consistent with the IS/OS and the PTOS in OCT?

Cone Structure

In this series of MacTel type 2 patients, cone spacing was normal in nearly all sites with contiguous and unambiguous arrays of cones. Specifically, the cones that regained visibility had normal spacing (two of two eyes). If these cones had migrated into their respective lesions, there would have been a corresponding increase in spacing (decrease in local density) as more normal cones moved into empty spaces to replace lost cones. In fact, the comprehensive image overlays for F1P1 (who had the best image quality) showed that at the two visits, in areas within 150 μm of where the cones became visible, the cone mosaic matched, cone-to-cone, indicating that the cones were not migrating at all.

Although the regrowth of entirely new cones is unlikely, it is possible for a cone to persist without the normal structures that give rise to the IS/OS and PTOS reflections. These reflections account for cone visibility not only on OCT, but also on AOSLO, images. It is therefore conceivable that cones with abnormal outer segments experience a loss of visibility but not necessarily a correspondingly complete loss of function. Indeed, two recent reports in the literature support the possibility of cones persisting in regions in which they are not visible on AOSLO or OCT. First, results from an AOSLO using a novel split-detection scheme has shown visible structures consistent with mosaics of inner segments in regions where standard confocal AOSLO imaging fails to show anything.[28] Second, a case report showed histologically normal-appearing cones within regions of IS/OS breaks, providing evidence that in MacTel type 2, breaks in the IS/OS junction may indicate conditions that disrupt the IS/OS cone reflectivity rather than cause photoreceptor death.[29] Neither of these analyses were done on our patients, however, as the new split-detector technology does not presently exist in our laboratory, and the histological analysis requires postmortem tissue.

Nevertheless, there are OCT findings that suggest the presence of a mostly intact cone array. Between the F1P1 and F2P1 study eyes, OCT B-scans revealed a consistent anatomical difference: in F1P1, the B-scans showed a relatively preserved ELM overlying a very transparent gap where the IS/OS and PTOS would normally be seen (Fig. 4A, white arrowheads), whereas in F2P1 they showed less evidence of an ELM where no IS/OS was visible (Fig. 4B, white arrowheads). The ELM, which consists of zonular adherences between Müller cell processes and photoreceptor inner segments, is believed to play an integral role in maintaining photoreceptor orientation and alignment.[30] Interestingly, the ELM band typically persists after IS/OS loss in other retinal degenerations, such as RP, choroideremia, and Stargardt disease.[30] Also, previous studies of postoperative recovery following macular hole closure, as well as retinal detachment repair, have found without
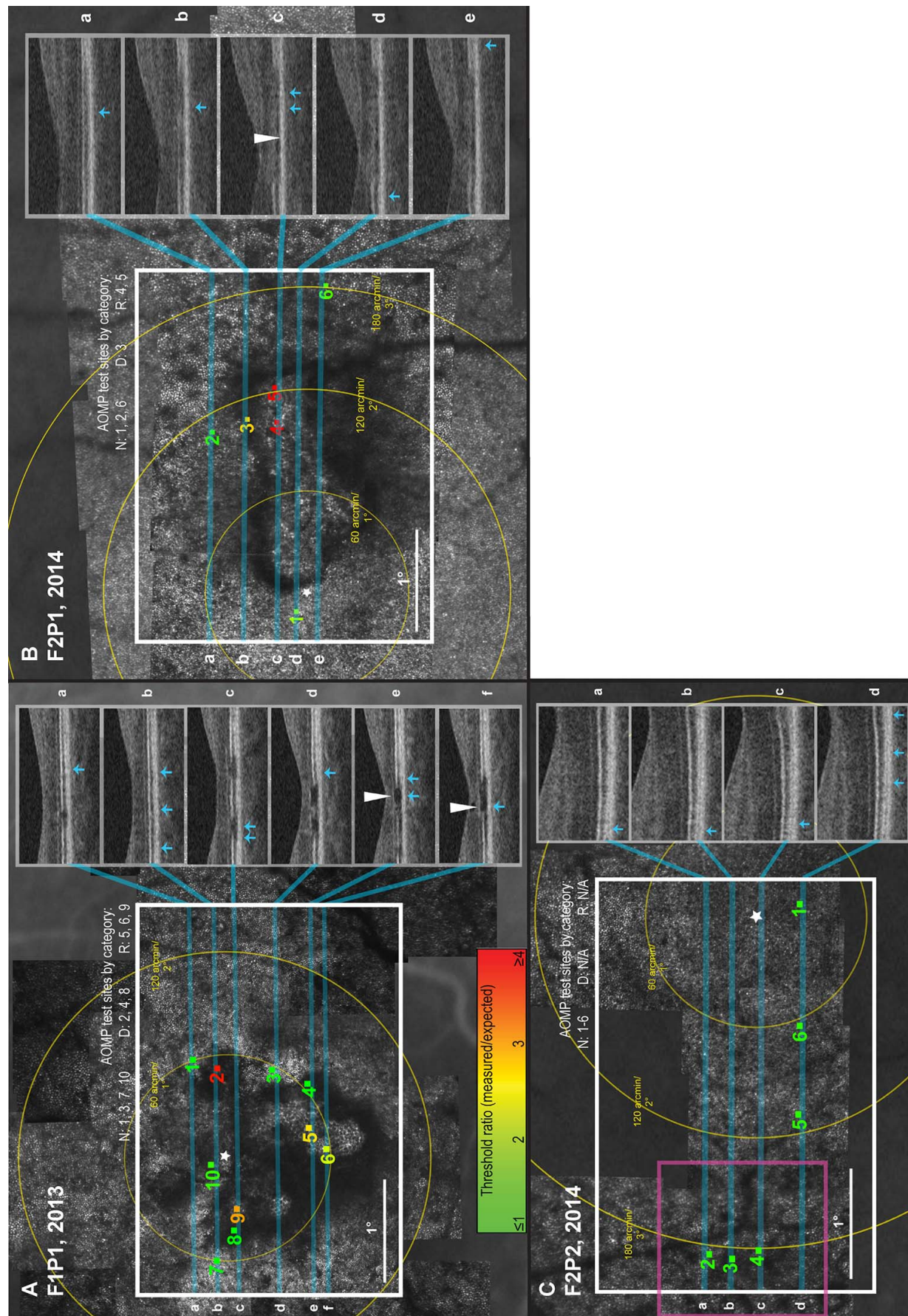
FIGURE 4. Cone structure and function in MacTel type 2 study eyes, shown via AOSLO montages, OCT scan lines, OCT B-scans, AOMP test site locations (*colored squares*, actual test stimulus size), and average AOMP threshold values (reported in au). Extent of threshold elevation compared with expected indicated by color. *White stars* mark foveas. *Scale bar*: 1°. B-scans were scaled and registered with vasculature before miniaturization (33% original). Scans show retinal anatomy at AOMP test sites (*blue arrows*). (**A**) AOSLO: MacTel type 2 lesion with RPE cells (R sites) and dim areas (D sites). (**a–f**) OCT: IS/OS breaks appear to have overlying preserved ELM bands (*white arrows*); RPE areas correspond to definitive IS/OS breaks on B-scans. Dim areas correspond with a range of IS/OS findings: test site 9 corresponds to an unambiguous break; 2, 4, and 8 to a present but relatively weakly reflecting IS/OS. AOMP: Measureable threshold values (au ±1 SD) at RPE sites are less abnormal than value at D site 2. (**B**) AOSLO: Visible RPE mosaics and dimly reflecting regions. OCT: Concurrent IS/OS and ELM disruptions (*white arrow*) correspond to AOMP R sites (4, 5), whereas D site 3 colocalizes with a present but weakly reflective IS/OS. AOMP: R site thresholds exceed thresholds in normal-appearing and dim areas. (**C**) AOSLO: Shadows of inner retinal abnormalities (*pink rectangle*). OCT: No disruption of the IS/OS junction band or ELM band. AOMP: Thresholds increased with eccentricity, with site 3 elevated more than site 2 or 4.

exception that ELM restoration preceded that of the IS/OS junction and that no eyes experienced IS/OS restoration without complete ELM recovery.[30,31]

An intact ELM that is accompanied by a transparent gap in the IS/OS could indicate intralesion regions in which cones are present and retain most of their structure. These retinal imaging findings should be explored further as potential imaging biomarkers of disease severity, as well as imaging features that may affect cone recovery prognosis.

Cone Function

Visual sensitivity was found in both the D and R regions, providing further evidence of the presence of abnormal and nonvisualizable cones. In F1P1, the R site (locations 5, 6, and 9) values were only approximately 2-fold higher than expected, suggesting relatively preserved visual sensitivity at those locations with visible RPE cell mosaics. In this eye, the AOMP test site with the most abnormal threshold value was located at a D site (location 2), indicating better visual sensitivity at R sites with visible RPE cells than D sites with dimly visible cones. In F2P1, the two R sites (locations 4 and 5) produced the most elevated thresholds observed, but only location 4 had thresholds that exceeded the limits of the AOMP system (more than eight times higher than expected). These findings contradict conventional beliefs that visualization of RPE cell mosaics and the loss of IS/OS and PTOS reflectivity indicate absence of cones and a corresponding inability to perceive light.[32] Although it is very likely that there are many cases where this is true, it does not apply to the examples shown in this article.

The AOMP data from F1P1 and F2P1 indicate that the structural scaffolding of the ELM also may be integral to preserving cones that maintain their visual sensitivity in regions in which the IS/OS junction is disrupted. In other words, lesions with preserved ELM and corresponding inner segments may contain functional cones. The presence of measurable AOMP thresholds raises the possibility that such intralesion cones, instead of being truly absent, have abnormal scattering and/or waveguiding qualities that preclude their visibility on confocal AOSLO imaging.

It also is possible that the threshold values seen at AOMP R test sites (locations 5, 6, and 9 in F1P1) represent responses by more normal neighboring cones stimulated as a result of intraretinal scatter. However, given that a D site in F1P1 (location 2) showed a high threshold in the immediate vicinity of two N regions, and that R sites in F2P1 (locations 4 and 5) produced severely elevated thresholds despite being located at similar distances from normal-appearing cones, it is unlikely that scattered light contributed significantly to the relatively low threshold values observed in F1P1. Moreover, in a separate study using the same system on normal eyes, intraretinal scattering did not appear to contribute to the observed changes in retinal sensitivity of cone-sized stimuli placed between versus on individual cones.[33]

In conclusion, the OCT/AOSLO/AOMP findings demonstrate that in lesions with a preserved ELM and transparent gap where the IS/OS and PTOS are normally seen (F1P1), there may be cones with abnormal scattering characteristics that cause the appearance of focal cone loss. Over time, these cones may regain normal scattering characteristics and once again become observable with AOSLO and/or OCT. Such cones also appear to retain light sensitivity, albeit with elevated thresholds. In regions in which the ELM is less intact and where the space normally occupied by the IS/OS and PTOS is replaced with more diffusely scattering tissue, visual function is more disrupted. No recovery of cone visibility has been found in these regions, although we have tracked progression of only two patients. Taken together, the results of this article suggest a potential use for OCT, with or without other advanced imaging and testing technology, in identifying and quantifying regions of functional and recoverable cones in MacTel type 2 and possibly other diseases.
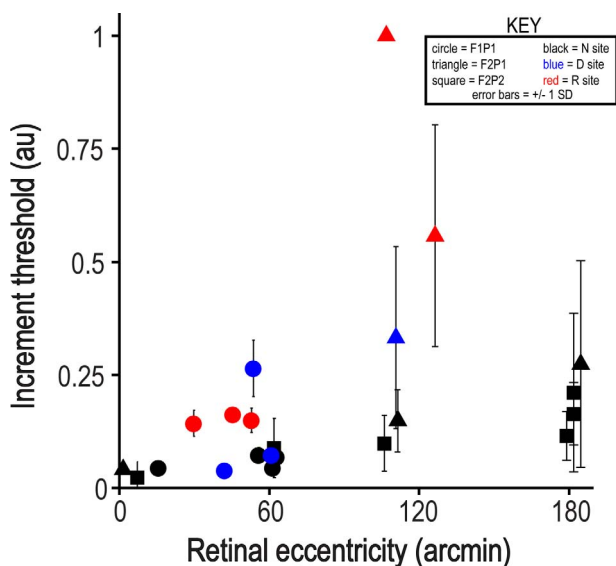
FIGURE 5. Adaptive optics MP thresholds from all three study eyes are shown. Thresholds at normal (N, *black*) locations increase with eccentricity and serve as comparison for thresholds at dim (D, *blue*) and RPE (R, *red*) sites.

References

1. Finger RP, Charbel Issa P, Fimmers R, Holz FG, Rubin GS, Scholl HP. Reading performance is reduced by parafoveal scotomas in patients with macular telangiectasia type 2. *Invest Ophthalmol Vis Sci*. 2009;50:1366–1370.

2. Gass JD, Blodi BA. Idiopathic juxtafoveolar retinal telangiectasis. Update of classification and follow-up study. *Ophthalmology*. 1993;100:1536–1546.

3. Gass JD, Oyakawa RT. Idiopathic juxtafoveolar retinal telangiectasis. *Arch Ophthalmol*. 1982;100:769–780.

4. Yannuzzi LA, Bardal AM, Freund KB, Chen KJ, Eandi CM, Blodi B. Idiopathic macular telangiectasia. *Arch Ophthalmol*. 2006;124:450–460.

5. Charbel Issa P, Gillies MC, Chew EY, et al. Macular telangiectasia type 2. *Prog Retin Eye Res*. 2013;34:49–77.

6. Sallo FB, Peto T, Egan C, et al. The IS/OS junction layer in the natural history of type 2 idiopathic macular telangiectasia. *Invest Ophthalmol Vis Sci*. 2012;53:7889–7895.

7. Klein R, Blodi BA, Meuer SM, Myers CE, Chew EY, Klein BE. The prevalence of macular telangiectasia type 2 in the Beaver Dam eye study. *Am J Ophthalmol*. 2010;150:55–62. e52.

8. Clemons TE, Gillies MC, Chew EY, et al. The National Eye Institute Visual Function Questionnaire in the Macular Telangiectasia (MacTel) Project. *Invest Ophthalmol Vis Sci*. 2008;49:4340–4346.

9. Clemons TE, Gillies MC, Chew EY, et al. Baseline characteristics of participants in the natural history study of macular telangiectasia (MacTel) MacTel Project Report No. 2. *Ophthalmic Epidemiol*. 2010;17:66–73.

10. Liang J, Williams DR, Miller DT. Supernormal vision and high-resolution retinal imaging through adaptive optics. *J Opt Soc Am A Opt Image Sci Vis*. 1997;14:2884–2892.

11. Dubra A, Sulai Y, Norris JL, et al. Noninvasive imaging of the human rod photoreceptor mosaic using a confocal adaptive optics scanning ophthalmoscope. *Biomed Opt Express*. 2011;2:1864–1876.

12. Roorda A, Romero-Borja F, Donnelly W III, Queener H, Hebert T, Campbell M. Adaptive optics scanning laser ophthalmoscopy. *Opt Express*. 2002;10:405–412.

13. Staurenghi G, Sadda S, Chakravarthy U, Spaide RF. Proposed lexicon for anatomic landmarks in normal posterior segment spectral-domain optical coherence tomography: the IN*OCT consensus. *Ophthalmology*. 2014;121:1572–1578.

14. Ooto S, Hangai M, Takayama K, et al. High-resolution photoreceptor imaging in idiopathic macular telangiectasia type 2 using adaptive optics scanning laser ophthalmoscopy. *Invest Ophthalmol Vis Sci*. 2011;52:5541–5550.

15. Ooto S, Hangai M, Takayama K, et al. Comparison of cone pathologic changes in idiopathic macular telangiectasia types 1 and 2 using adaptive optics scanning laser ophthalmoscopy. *Am J Ophthalmol*. 2013;155:1045–1057.e4.

16. Tuten WS, Tiruveedhula P, Roorda A. Adaptive optics scanning laser ophthalmoscope-based microperimetry. *Optom Vis Sci*. 2012;89:563–574.

17. Duncan JL, Zhang Y, Gandhi J, et al. High-resolution imaging with adaptive optics in patients with inherited retinal degeneration. *Invest Ophthalmol Vis Sci*. 2007;48:3283–3291.

18. Merino D, Duncan JL, Tiruveedhula P, Roorda A. Observation of cone and rod photoreceptors in normal subjects and patients using a new generation adaptive optics scanning laser ophthalmoscope. *Biomed Opt Express*. 2011;2:2189–2201.

19. Talcott KE, Ratnam K, Sundquist SM, et al. Longitudinal study of cone photoreceptors during retinal degeneration and in response to ciliary neurotrophic factor treatment. *Invest Ophthalmol Vis Sci*. 2011;52:2219–2226.

20. Ratnam K, Carroll J, Porco TC, Duncan JL, Roorda A. Relationship between foveal cone structure and clinical measures of visual function in patients with inherited retinal degenerations. *Invest Ophthalmol Vis Sci*. 2013;54:5836–5847.

21. Wald G. The receptors of human color vision. *Science*. 1964;145:1007–1016.

22. Curcio CA, Sloan KR, Kalina RE, Hendrickson AE. Human photoreceptor topography. *J Comp Neurol*. 1990;292:497–523.

23. Arathorn DW, Yang Q, Vogel CR, Zhang Y, Tiruveedhula P, Roorda A. Retinally stabilized cone-targeted stimulus delivery. *Opt Express*. 2007;15:13731–13744.

24. Atchison DA, Smith G. Chromatic dispersions of the ocular media of human eyes. *J Opt Soc Am A Opt Image Sci Vis*. 2005;22:29–37.

25. Harmening WM, Tiruveedhula P, Roorda A, Sincich LC. Measurement and correction of transverse chromatic offsets for multi-wavelength retinal microscopy in the living eye. *Biomed Opt Express*. 2012;3:2066–2077.

26. Artes PH, Iwase A, Ohno Y, Kitazawa Y, Chauhan BC. Properties of perimetric threshold estimates from Full Threshold, SITA Standard, and SITA Fast strategies. *Invest Ophthalmol Vis Sci*. 2002;43:2654–2659.

27. Rodieck RW. The density recovery profile: a method for the analysis of points in the plane applicable to retinal studies. *Vis Neurosci*. 1991;6:95–111.

28. Scoles D, Sulai YN, Langlo CS, et al. In vivo imaging of human cone photoreceptor inner segments. *Invest Ophthalmol Vis Sci*. 2014;55:4244–4251.

29. Powner MB, Gillies MC, Zhu M, Vevis K, Hunyor AP, Fruttiger M. Loss of Muller's cells and photoreceptors in macular telangiectasia type 2. *Ophthalmology*. 2013;120:2344–2352.

30. Mitamura Y, Mitamura-Aizawa S, Katome T, et al. Photoreceptor impairment and restoration on optical coherence tomographic image. *J Ophthalmol*. 2013;2013:518170.

31. Ooka E, Mitamura Y, Baba T, Kitahashi M, Oshitari T, Yamamoto S. Foveal microstructure on spectral-domain optical coherence tomographic images and visual function after macular hole surgery. *Am J Ophthalmol*. 2011;152:283–290.e1.

32. Roorda A, Zhang Y, Duncan JL. High-resolution in vivo imaging of the RPE mosaic in eyes with retinal disease. *Invest Ophthalmol Vis Sci*. 2007;48:2297–2303.

33. Harmening WM, Tuten WS, Roorda A, Sincich LC. Mapping the perceptual grain of the human retina. *J Neurosci*. 2014;34:5667–5677.